Biochimica et Biophysica Acta, 1060 (1991) 13–24

ADONIS 000527289100215B

BBABIO 43472

Ultrafast pump-probe spectroscopy of bacteriochlorophyll *c* antennae in bacteriochlorophyll *a*-containing chlorosomes from the green photosynthetic bacterium *Chloroflexus aurantiacus*

Su Lin, Herbert Van Amerongen and Walter S. Struve

Ames Laboratory-USDOE and Department of Chemistry, Iowa State University, Ames, IA (U.S.A.)

(Received 14 March 1991)

Key words: Antenna; Bacterial photosynthesis; Bacteriochlorophyll; Chlorosome; Pump-probe spectroscopy; Ultrafast spectroscopy; (*C. aurantiacus*)

Time-dependent isotropic and anisotropic absorption difference profiles have been obtained with 2 ps resolution for the (BChl) bacteriochlorophyll *c* antenna in BChl *a*-containing chlorosomes from the green photosynthetic bacterium *Chloroflexus aurantiacus*. The isotropic absorption difference spectra are bipolar; they are dominated by excited state absorption at wavelengths < 725 nm, and by ground state photobleaching at wavelengths > 735 nm. The entire isotropic spectrum exhibits a dynamic blue shift over approx. 4 nm with a time constant of approx. 7 ps. All of these phenomena are rationalized in terms of a linear exciton model that resembles the theory of *J*-aggregates. In this theory, the occurrence of the dynamic blue shift corresponds to relaxation between Q_y excitation components; it cannot readily be explained using a model that assumes that the excitations are localized on single chromophores within 1 ps. The anisotropic decay times, resolved here for the first time with our 2 ps fwhm instrument function, are approx. 7 ± 1 ps at 720 nm and 4 ± 1 ps at 740 nm. The residual anisotropy $r(\infty)$ is 0.32 ± 0.02 at 740 nm, which is in good agreement with fluorescence and linear dichroism measurements. These anisotropy functions initialize to 0.4 within error, indicating that subpicosecond depolarization is not prevalent.

Introduction

Chlorosomes constitute the principal light-harvesting antennae of the green photosynthetic bacterium *Chloroflexus aurantiacus*. These ellipsoidal bodies (of dimensions $100 \times 30 \times 12$ nm) comprise rodlike elements containing BChl *c* pigments [1]. Each chlorosome contains several thousand BChl *c* chromophores, in addition to a significant amount of carotenoids [2]; the ratio of reaction centers to chlorosomes in this bacterium has been estimated to be about 50. Electronic excitation created by light absorption in the carotenoids and the BChl *c* pigments (whose absorption band maximum is at ~ 740 nm) is transferred to the reaction centers via B808-866 BChl *a* complexes and BChl *a* complexes that absorb at approx. 795 nm [3–6]. The B808-866 complexes and the reaction centers are located in the cytoplasmic membrane, while the BChl *a* antenna is believed to occupy a baseplate that connects the chlorosome to the membrane.

It is well documented that ultrafast electronic energy transfer (EET) occurs between the BChl *c* and BChl *a* assemblies. Fluorescence decays emitted by these chlorosomes are generally multiexponential [4–6], and two groups have isolated BChl *c* lifetimes through global analysis techniques [5,6]. Mimuro et al. [4] measured a BChl *c* decay time of approx. 16 ps for selectively excited BChl *c* pigments in whole cells of *Chloroflexus aurantiacus*. Similarly, Müller et al. [5] and Causgrove et al. [6] used global analyses to obtain a 16–19 ps decay time for BChl *c* emission in whole cells; it was ascertained [5,6] that this is mirrored by a corresponding risetime in BChl *a* emission. Somewhat faster EET is apparently observed in isolated BChl *a*-containing chlorosomes. For example, Holzwarth et al. [7] found that the decay-associated fluorescence

Abbreviations: BChl, bacteriochlorophyll; EET, electronic energy transfer; DAS, decay-associated fluorescence; CD, circular dichroism.

Correspondence: W.S. Struve, Ames Laboratory-USDOE and Department of Chemistry, Iowa State University, Ames, IA 50011, U.S.A.

spectrum (DAS) of BChl *a*-containing chlorosomes exhibits at least two decay components (11 and 27 ps) which are concentrated at BChl *c* fluorescence wavelengths (750–760 nm). The (dominant) 11 ps component, which was mirrored by a risetime component at BChl *a* fluorescence wavelengths, was attributed to BChl *c* → BChl *a* EET. The origin of the 27 ps component, which exhibited a secondary maximum near 795 nm, was unclear. In a pump-probe study of BChl *a*-containing chlorosomes, Miller et al. [8] characterized three lifetime components in the 750 nm isotropic photobleaching decay; 11 ps (76%), 39 ps (19%) and 350 ps (5%). The first two of these clearly resemble the BChl *c* DAS fluorescence components identified by Holzwarth et al.; the longest lifetime may correspond to unassigned long-wavelength components that have been observed by several groups [4–7]. Holzwarth et al. also identified a 5 ± 2 ps DAS component in BChl *a*-free chlorosomes that exhibited positive amplitude at short BChl *c* emission wavelengths, and negative amplitude at longer BChl *c* wavelengths [7]. Two possible interpretations of this intriguing behavior were (a) downhill EET between distinct BChl *c* spectral forms (or 'pigment pools'), and (b) relaxation between different BChl *c* exciton components. Polarized pump-probe studies [8] indicate that the anisotropy of transient photobleaching in BChl *a*-containing chlorosomes reaches an asymptotic value ($r(\infty) = 0.20 \pm 0.05$ at 750 nm) in less than approx. 10 ps, the experimental time resolution. In summary, while there is considerable agreement on the phenomenological dynamics of EET between the BChl *c* and BChl *a* antennae, relatively little is understood about the mechanisms of internal EET within the BChl *c* assemblies.

Absorption, linear dichroism, electron microscopy and fluorescence experiments have all shown that the organization of BChl *c* chromophores is very similar in BChl *a*-containing and BChl *a*-free chlorosome preparations [7,9,10]. While BChl *c* circular dichroism (CD) spectra of chlorosomes are unreproducible even for fresh preparations [10], no systematic differences appear here between BChl *a*-containing and BChl *a*-free chlorosomes. Linear dichroism measurements show that the BChl *c* pigments are organized with their Q_y absorption transition moments at an average angle of 17° with respect to the chlorosome long axis [10,11]. Polarized fluorescence studies of oriented chlorosomes in compressed gels [11] similarly show that the corresponding emission transition moments are aligned at 17° from the chlorosome axis. This agreement between the measured absorption and fluorescence anisotropies indicates that the excited state depolarization proceeds on a time scale far shorter than the BChl *c* fluorescence lifetime. This is confirmed by the dynamic linear dichroism studies of Gillbro and coworkers [8] and Fetisova et al. [13], who reported unresolvably fast depolarization in pump-probe and fluorescence experiments, respectively.

A unique feature of the BChl *c* pigment organization in chlorosomes in its close spectroscopic similarity to BChl *c* aggregates that spontaneously form from the monomers in solution. This 'self-aggregating' property, which has potential utility in the construction of model antenna in artificial photosynthesis, has been extensively studied [10–22]. The in vitro BChl *c* aggregates, like the BChl *c* assemblies in chlorosomes, exhibit absorption bands red-shifted by 1400 cm^{-1} from the monomer band; they also share similar CD as well as ultrafast fluorescence decay times. The latter property is reminiscent of exciton-coupled *J*-aggregates [23], in which the radiative lifetime of the lowest exciton component is shorter than that of the monomer by a factor of approximately n, the number of exciton-coupled monomers in the aggregate [24]. However, the presence of circular dichroism [10] indicates that the BChl *c* transition moments in chlorosomes cannot be parallel as in *J*-aggregates, but must at least precess from chromophore to chromophore through some azimuthal angle about the aggregate axis. The role of protein complexing in the BChl *c* aggregation is unclear. Griebenow et al. [10] reported isolation of BChl *a*-free chlorosomes containing essentially no protein, with BChl *c* spectroscopic properties closely resembling those of BChl *a*-containing chlorosomes. Following a similar isolation procedure, Eckhardt et al. [25] obtained modified chlorosomes containing large amounts of c-protein in addition to BChl pigments. They concluded that c-protein is localized in the interior of these chlorosomes, and thus that the protein may be structurally involved in the organization of the BChl *c* chromophores.

In this work, we report an isotropic and polarized pump-probe study of the BChl *c* absorption band (715–755 nm) in BChl *a*-containing chlorosomes from *Chloroflexus aurantiacus*. Strong excited-state absorption is observed at the shorter wavelengths (≤ 730 nm), while the transients at longer wavelengths are dominated by apparent photobleaching of ground-state absorption. This bipolarity is similar to that observed earlier in absorbance difference spectra of *Chlorobium limicola* and *Chloroflexus aurantiacus* chlorosomes excited with 35 ps laser pulses at 532 nm [26]. The 2 ps resolution of the present study reveals that the entire isotropic pump-probe spectrum blue-shifts dynamically during the first few picoseconds. The present time resolution also permits accurate measurement of the anisotropic decay times at 720 and 740 nm. Our results are discussed in the context of exciton theories for ground and excited-state absorption in linear aggregates, with a view toward interpreting the isotropic spectra and their early-time behavior.

Materials and Methods

The BChl *a*-containing chlorosomes, generously provided by Dr. Alfred R. Holzwarth at Max Planck Institut, Mülheim, were isolated from *Chloroflexus aurantiacus* following the method of Feick et al. [27]. Steady-state absorption spectra, measured on a Perkin-Elmer 3B spectrophotometer, exhibited the characteristic absorption maximum and shoulder (~ 740 nm and ~ 795 nm [28]) of the BChl *c* and BChl *a* antennae. The chlorosomes were stored near 0 °C in the dark and used as needed. In pump-probe experiments, samples were circulated at room temperature through a Starna 49-C1 1 mm path length flow cell at 23 cm/s to minimize laser photooxidation. The sample optical absorbance at 740 nm was typically 0.35.

The lasers and pump-probe apparatus have been described previously [29]. A hybrid mode-locked dye laser (pyridine 2 laser dye, DDI saturable absorber) was pumped using 532 nm SHG pulses (~ 1 W average power) from a Coherent Antares 76-s Nd:YAG cw mode-locked laser. Dye laser pulses typically exhibited autocorrelations with approx. 2 ps fwhm, and were tunable from 685 to 765 nm. Pump-probe signals were detected using an RF multiple modulation scheme: the pump and probe beams were modulated at 6.5 and 0.5 MHz, and the 7.0 MHz sum frequency component in the transmitted probe beam was detected using a modified Drake R-7A radio receiver. The probe beam polarization was fixed at 45 ° from the vertical using a calcite Glan-Thompson prism; the pump polarization could be alternated among parallel, perpendicular, and magic-angle (54.7 °) with respect to the probe polarization. The variable pump pulse time delay was provided by a Micro-Controle UT100125PP translation stage. An EG&G FOD-100 silicon photodiode detected the probe beam. The radio receiver's signal-bearing 50 kHz intermediate frequency was routed to a Stanford Research Systems SR510 lock-in amplifier. Time-dependent pump-probe profiles were accumulated in a DEC MINC-23 computer, and were analyzed with a nonlinear least-squares convolute-and-compare algorithm in a DEC VAXstation 2000.

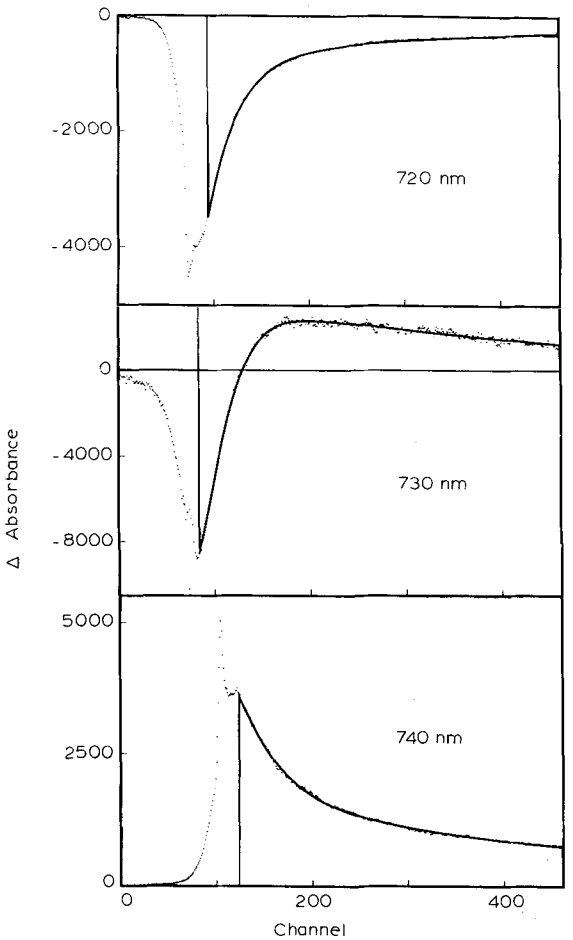

Fig. 1. Isotropic absorption difference profiles at 720, 730 and 740 nm. Time calibration is 0.1 ps/channel. Negative and positive signals correspond to excited state absorption and ground state photobleaching, respectively. Continuous curves show optimized convolutions of laser autocorrelation function with biexponential decay model. Final parameters for biexponential and triexponential fits to these and all other isotropic profiles are given in Table I. The profiles at different wavelengths are not mutually normalized.

The number of photons absorbed per laser pulse in the region of overlap between the pump and probe pulses was typically $3.6 \cdot 10^6$ at 740 nm. Since the number of BChl *c* chromophores in this volume was $\sim 3.7 \cdot 10^8$, one out of every 100 BChl *c* chromophores was typically excited by each pump pulse at this wavelength; fewer than this were excited at the other wavelengths.

Action spectra were obtained by probing the wavelength dependence of the optical density transient at a fixed time delay, and were normalized to the square of the laser beam intensity at each wavelength.

Results

Isotropic decay

Time-dependent optical density transients were obtained at wavelengths where the ground-state absorption is dominated by the BChl *c* Q_y band, 715–755 nm. The observed decays are strongly wavelength-dependent; the trends are illustrated by the profiles shown in Fig. 1 for 720, 730 and 740 nm. The positive-going isotropic signal at 740 nm corresponds to photobleaching decay arising from ground-state recovery, combined with stimulated emission (vide infra). It is clearly not single-exponential, since at least two decay components are required to describe its kinetics. Table I lists the final fitting parameters for optimized bi- and triexponential model functions at all of the wavelengths studied. The negative-going isotropic signal at 720 nm arises from excited-state absorption, and ex-

hibits considerably more rapid decay kinetics overall than the ground-state recovery at 740 nm (cf. Fig. 1 and Table I). The isotropic signal at 730 nm shows a combination of excited-state absorption at early times and photobleaching decay at long times. The optical density transients metamorphose rapidly with wavelength between 728 and 735 nm, where the difference absorption spectra reverse sign (vide infra). Hence, the ± 1 nm uncertainty in the laser wavelength rendered the multiexponential fitting parameters for the transitional wavelengths in Table I less reproducible than those at the other wavelengths, where the isotropic decay is monotonic.

Biexponential fits to the isotropic decays at wavelengths below 730 nm are dominated (> 90%) by a short component with lifetime approx. 3–4 ps. An additional component, characterized by a lifetime of typically 40 ps, becomes substantial (> 10%) at wavelengths longer than 735 nm, rendering these long-wavelength decays slower than at the shortest wavelengths. Triexponential fits do not greatly improve the optimized χ^2, as even the comparatively high signal-to-noise ratios in the present pump-probe transients do not approach those of time-correlated photon-counting experiments. However, the optimized triexponential fits do yield different sets of lifetimes than the biexponential fits, as shown in Table I. In particular, the 10–15 ps intermediate lifetime component that emerges in triexponential fits at wavelengths $\geq$ 740 nm are similar to BChl *c* lifetimes reported in fluorescence and long-wavelength pump-probe experiments [7,8]. Both the biexponential and triexponential fits at wavelengths longer than 735 nm yield a large-amplitude fast component of lifetime 3–4 ps, which has not been reported in other time-resolved fluorescence or pump-probe experiments – presumably owing to their coarser time resolution. These lifetimes (like the short lifetime component at wavelengths < 725 nm) were reproducible to within ± 0.5 ps, provided the laser pulse autocorrelation width was maintained at less than 2 ps fwhm.

TABLE I

Fitting parameters from biexponential and triexponential analyses of isotropic BChl c decays [a]

Wavelength (nm)	$\tau_1(A_1)$	$\tau_2(A_2)$	$\tau_3(A_3)$
715	3.25 (−0.93)	40.2 (−0.07)	
720	3.23 (−0.95)	39.6 (−0.05)	
725	3.01 (−0.98)	30.2 (−0.02)	
731	1.15 (−0.51)	48.4 (0.49)	
735	3.80 (0.74)	40.1 (0.26)	
740	4.27 (0.72)	44.2 (0.28)	
745	4.18 (0.84)	41.5 (0.16)	
750	4.35 (0.89)	41.9 (0.11)	
755	3.49 (0.81)	34.2 (0.19)	
715	2.05 (−0.69)	5.76 (−0.25)	66.6 (−0.06)
720	1.41 (−0.64)	4.88 (−0.30)	63.5 (−0.06)
725	1.87 (−0.72)	5.11 (−0.26)	82.9 (−0.02)
728	1.31 (−0.58)	3.45 (−0.41)	55.1 (0.02)
731	1.17 (−0.47)	1.22 (−0.06)	48.2 (0.47)
735	3.44 (0.56)	20.3 (0.29)	110.0 (0.15)
740	3.48 (0.63)	15.9 (0.25)	157.0 (0.12)
745	3.21 (0.83)	12.2 (0.13)	158.0 (0.04)
750	2.95 (0.74)	10.6 (0.22)	49.8 (0.04)
755	2.55 (0.71)	12.0 (0.22)	235.0 (0.06)

[a] All lifetimes are in ps. The sum of absolute values of preexponential factors is normalized to unity.

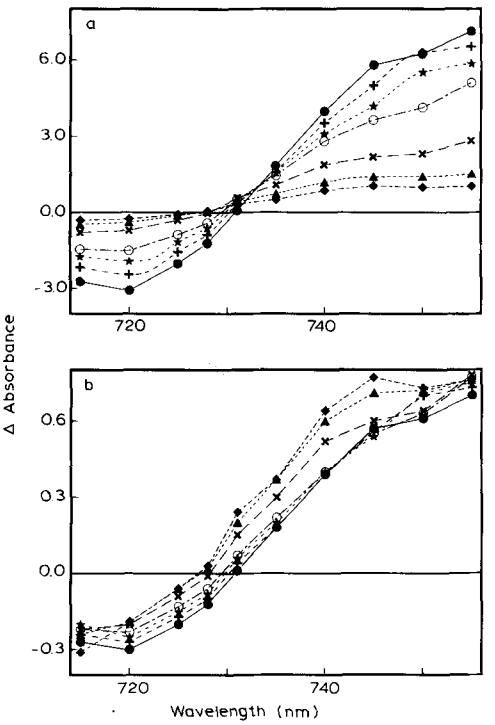

Fig. 2. Difference absorption spectra for fixed time delays, reconstructed from isotropic time-dependent profiles obtained at ten wavelengths from 715 to 755 nm. (a) Spectra with actual relative magnitudes at different time delays; the latter are (from top to bottom at the right-hand side) 2, 3, 4, 5, 10, 20 and 50 ps. (b) The same spectra normalized to the respective lock-in amplifier signal ranges.

The corresponding time-resolved absorption spectra are shown in Fig. 2. Spectra obtained by reconstruction from the isotropic absorbance transients obtained at different wavelengths were contrasted with those obtained directly by scanning the laser wavelength at a series of fixed time delays; the results obtained either way were essentially identical. Fig. 2a gives the reconstructed absorption spectra for chlorosomes excited at wavelengths between 715 and 755 nm. These emphasize the bipolarity of the spectra, which show photobleaching and excited-state absorption at the longer and shorter wavelengths, respectively. Both of these signals tend towards null at long times. A different perspective is offered in Fig. 2b, in which each of the absorption spectra has been normalized to the total signal range used in the lock-in amplifier. This representation emphasizes that the spectra exhibit a dy-

namic blue shift during the observed window of approx. 50 ps. This blue shift can be most accurately characterized by the wavelength position of the zero-crossing point interpolated between the nearest-neighbor data points in the photobleaching and excited-state absorption regions. This migrates from ~ 731 nm to ~ 727 nm during the first 50 ps. The zero-crossing wavelength is plotted against time in Fig. 3; analysis shows that this migration is well characterized by a single-exponential lifetime of ~ 7 ps, as the corresponding semilogarithmic plot (not shown) is essentially linear.

Anisotropic decays

There were evaluated by computing the anisotropy decay function $r(t)$ point by point from the polarized absorbance transients via

$$r(t) = \frac{\Delta A_{\parallel}(t) - \Delta A_{\perp}(t)}{\Delta A_{\parallel}(t) + 2\Delta A_{\perp}(t)} \quad (1)$$

Typical anisotropy decays obtained in this way at 720 and 740 nm are shown in Fig. 4, along with their optimized single-exponential fits. Both of these decays initialize to 0.4 within error, so that the present time resolution encompasses essentially all of the observed anisotropy decay. The anisotropic lifetime are approx. 7 ± 1 ps at 720 nm and 4 ± 1 ps at 740 nm; these were highly reproducible when the laser pulse autocorrelation fwhm was approx. 2 ps or shorter. The respective residual anisotropies $r(\infty)$ at long times are of interest because they can be compared with independent measurements by other groups; we find $r(\infty) = 0.24 \pm 0.02$ (720 nm) and 0.32 ± 0.02 (740 nm). If the distribution of BChl *c* transition moments is rotationally symmetric about the chlorosome long axis, the latter value corresponds to $\langle P_2(\cos \theta_\mu) \rangle = 0.89 \pm 0.03$ at 740 nm, i.e., $\theta_\mu \sim 17°$. Here, θ_μ is the angle formed between the absorption transition moment and the symmetry axis. The latter value is in excellent agreement with recent linear dichroism measurements of $\langle P_2(\cos \theta_\mu) \rangle$ at 740 nm, 0.90 ± 0.04 [10] and 0.87 ± 0.04 [11]; it is somewhat higher than the value 0.70 ± 0.09 (corresponding to $r(\infty) = 0.20 \pm 0.05$) obtained in the 750 nm pump-probe experiment [8]. Our 740 nm value also agrees with the result $(\langle P_2(\cos \theta_\mu) \rangle \langle P_2(\cos \theta_\nu) \rangle)^{1/2} = 0.89 \pm 0.01$ determined by Fetisova et al. [13], where θ_ν is the angle between the fluorescence transition moment and the aggregate axis. (It is not clear that the latter value can be directly compared with ours, since it is derived from observation of 730 nm fluorescence excited at 711 nm.) Similarly, a steady-state fluorescence polarization measurement on oriented chlorosomes [12] gives $\langle P_2(\cos \theta_\nu) \rangle = 0.89 \pm 0.02$. A slightly lower residual polarization was obtained by van Dorssen et al. ($p = 0.35$, or $(\langle P_2(\cos \theta_\mu) \rangle \langle P_2(\cos \theta_\nu) \rangle)^{1/2} = 0.81$) from steady-state fluorescence measurements on isolated chlorosomes [30].

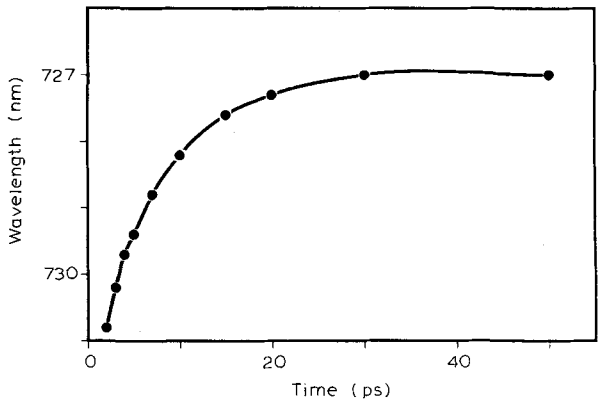

Fig. 3. Plot of zero-crossing wavelength of difference absorption spectra (Fig. 2) versus time delay.

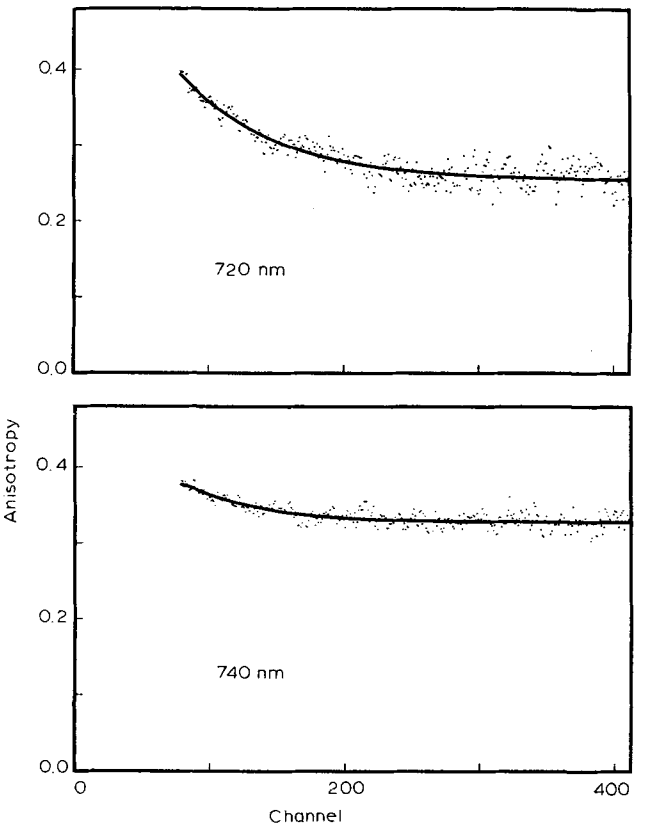

Fig. 4. Anisotropy functions $r(t)$ for pump-probe transients at 720 nm and 740 nm. Channel calibration is 0.1 ps/channel. Continuous curves show optimized convolutions of laser autocorrelation functions with single-exponential decay model for $r(t)$. The anisotropy decay times are 7 ± 1 ps and 4 ± 1 ps at 720 and 740 nm, respectively.

Discussion

The most distinguishing feature of the isotropic decays and their corresponding spectra is their bipolarity, which stems from the presence of excited state absorption at the shorter wavelengths. Our spectra in Fig. 2 were anticipated by qualitatively similar absorbance

difference spectra reported for chlorosomes from *C. limicola* and *C. aurantiacus* [26]. Such intense excited state absorption, occurring at wavelengths that nearly overlap the ground state spectrum, appears to be unrelated to the excited state absorption of BChl *c* monomers. It can arise in consequence of strong excitation coupling between monomers in the rodlike BChl *c* elements. Hence, we preface the discussion of our isotropic decays and spectra by describing an exciton model for the excited state electronic structure in linear aggregates in which all N chromophores experience identical exciton couplings with their nearest neighbors. The N singly excited exciton states at this level of approximation are formed by diagonalizing the electronic Hamiltonian in the basis of n localized excited states

$$\Phi_i^{(1)} = \phi_i^* \prod_{i \neq j}^{N-1} \phi_j \tag{2}$$

in a degenerate perturbation treatment. Here ϕ_i and ϕ_i^* denote the BChl *c* monomer ground and Q_y electronic states, respectively. In the presence of uniform exciton couplings β between nearest-neighbor chromophores with Q_y state energy α, the N energy eigenvalues for the singly excited exciton states become [23]:

$$E_i^{(1)} = \alpha \pm 2\beta \cos\left(\frac{\pi}{N+1}\right),\ \alpha \pm 2\beta \cos\left(\frac{2\pi}{N+1}\right),$$

$$\alpha \pm 2\beta \cos\left(\frac{3\pi}{N+1}\right), \ldots, (0) \tag{3}$$

where the eigenvalue 0 exists if N is odd. The corresponding expansion coefficients c_{ij} for these zeroth-order exciton states

$$\Psi_i^{(1)} = \sum_{j=1}^{N} c_{ij} \Phi_j^{(1)} \tag{4}$$

are given by the analytic expression

$$c_{ij} = \left(\frac{2}{N+1}\right)^{1/2} \sin\left(\frac{ij\pi}{N+1}\right) \tag{5}$$

The intensities of the absorption bands arising from ground state absorption to the singly excited exciton components Ψ_i are then computed from

$$I_{ik} = \left(\sum_{j=1}^{n} c_{ij}\mu_{jk}\right)^2, k = x, y, z \tag{6}$$

via $I_i = I_{ix} + I_{iy} + I_{iz}$. While Eqns. 3 and 5 for the eigenvalues and expansion coefficients are identical to those for *J*-aggregates [23], the intensities of the exciton component bands must be somewhat different for BChl *c* aggregates: the monomer Q_y transition moment directions μ are all parallel in *J*-aggregates, whereas the BChl *c* CD spectra in chlorosomes indicate the presence of a chiral architecture. For definiteness, we adopt the simplest model, in which the BChl *c* Q_y orientations in chlorosomes are given by

$$\mu_j = \begin{pmatrix} \sin\theta \cos(j\phi) \\ \sin\theta \sin(j\phi) \\ \cos\theta \end{pmatrix} \tag{7}$$

In this model, the angle θ between the transition moments and the linear aggregate axis would be approx. 17° according to linear dichroism experiments if the aggregate and chlorosome axes are parallel [10,11], but the azimuthal precession angle ϕ is unknown. In the special case of *J*-aggregates ($\beta < 0$, $\phi = 0°$), more than 80% of the total electric dipole strength is concentrated in the transition to the lowest exciton component, with the consequences that (a) the N-aggregate's absorption spectrum is sharply peaked and red-shifted with respect to the monomer spectrum and (b) the radiative lifetime of the lowest exciton component is on the order of τ_F/N, where τ_F is the monomer radiative lifetime. To the same level of approximation, the doubly excited exciton states (which are required for modeling excited state absorption in the wavelength region of the ground state absorption) can be expanded in the $N(N-1)/2$ localized basis functions

$$\Phi_{ij}^{(2)} = \phi_i^* \phi_j^* \prod_{k \neq ij}^{N-2} \phi_k \text{ for } j > i;\ i = 1, \ldots, N-1 \tag{8}$$

$$\Psi_n^{(2)} = \sum_{ij} b_{nij} \Phi_{ij}^{(2)} \tag{9}$$

The $N(N-1)/2$ energy eigenvalues of the degenerate perturbation problem in this basis are

$$E_n^{(2)} = 2\alpha + 2\beta\left[\cos\left(\frac{p\pi}{N+1}\right) + \cos\left(\frac{q\pi}{N+1}\right)\right] \tag{10}$$

where p runs from 1 to $(N-1)$ and q runs from $(p+1)$ to N for given p. These eigenvalues and the corresponding eigenvectors (not shown) may be used along with the assumed transition moment directions (e.g., Eqn. 7) to complete the excited state absorption spectrum that arises from transitions between pairs of single and doubly excited exciton components $\Psi_i^{(1)}$ and $\Psi_n^{(2)}$. Some of the principal features of the resulting exciton transitions are illustrated for the idealized case of a *J*-aggregate with $N = 5$ in Fig. 5. Here, the five singly excited exciton components have energies $\alpha \pm 1.732\beta$, $\alpha \pm \beta$ and 0; the ten doubly excited components have energies $2\alpha \pm 2.732\beta$, $2\alpha \pm 1.732\beta$, $2\alpha \pm \beta$, $2\alpha \pm 0.732\beta$ and 0 (the latter level being doubly degenerate). The ground state Q_y absorption is strongly dominated by the transition to the lowest-energy singly

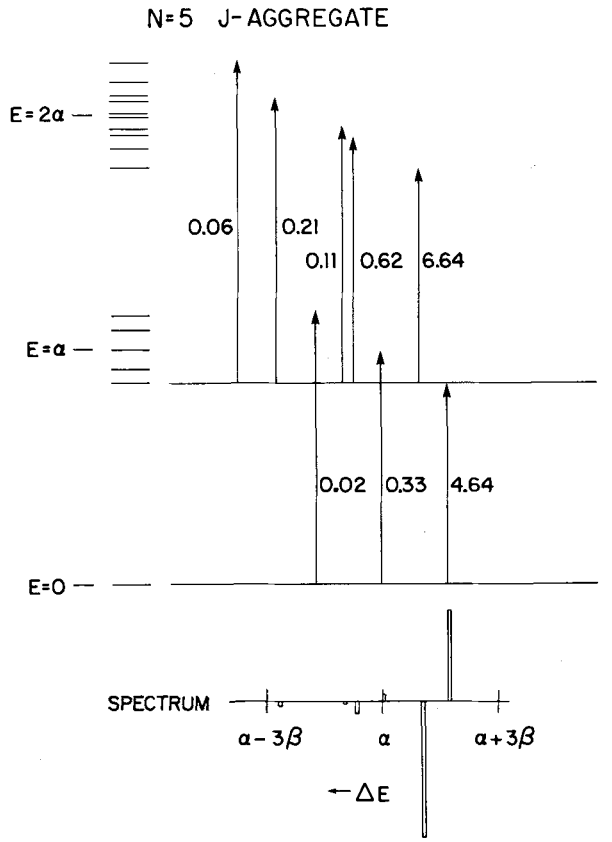

Fig. 5. Schematic energy level diagram for singly and doubly excited exciton states in a J-aggregate with $N = 5$. Arrows show allowed transitions from the ground state and from the lowest singly excited exciton component; numbers denote relative intensities. (These intensities sum up to $N = 5$ for ground state transitions to the singly excited exciton components, and to $N(N-1) = 20$ for all transitions between singly and doubly excited exciton components; only the transitions from the lowest singly excited component are shown for clarity.) Resulting spectrum is shown at bottom, where positive and negative signals indicate photobleaching and excited state absorption, respectively.

excited component, which has energy $\alpha + 1.732\beta$ for $N = 5$. Nearly all of the electric dipole strength for subsequent transitions to the doubly excited exciton components is concentrated in the transition to the lowest component, which has energy $2\alpha + 2.732\beta$. This results in a significant blue shift of 0.732β between the ground-state and excited-state absorption spectra; for comparison, the red shift of the aggregate's ground state absorption spectrum relative to that of the monomer is 1.732β. Hence, the simple J-aggregate model already predicts the gross shape of the absorption difference spectra in Fig. 2, where ground-state photobleaching and excited-state absorption predominate at the longer and shorter wavelengths, respectively. For large N, the dipole strengths for ground state absorption are less sharply concentrated in the transition to the lowest exciton component. In this limit, the fraction of the total dipole strength for ground state absorption to the lowest excitation component is $8/\pi^2 = 0.81$; the corresponding fraction for absorption to the ith exciton component ($i = 1$ being the lowest-energy component) is $8/i^2\pi^2$ for odd i and 0 for even i. This results in a J-aggregate ground state absorption spectrum that is shifted by essentially 2β from the monomer spectrum when N is large.

Stimulated emission transitions, which are not considered in Fig. 5, inevitably contribute to the total absorption difference signal. In a two-level system, the Einstein coefficients B_{12} and B_{21} for absorption and stimulated emission are equal if the level degeneracies are the same. In transitions between two electronic singlet states, the pertinent Einstein coefficients are B_{0v}, for absorption from the vibrationless ground state to vibrational state v' in the excited state, and $B_{v''0}$ for stimulated emission from the vibrationally relaxed excited state to vibrational state v'' in the electronic ground state. These obey the sum rule

$$\sum_{v'} B_{0v'} = \sum_{v''} B_{v''0}$$

This implies that the integrated spectra for photobleaching and stimulated emission between a given pair of electronic states (e.g., the ground state and a single excited exciton component) will be equal. The stimulated emission signal exhibits the same sign as the photobleaching component in absorption difference spectra; like the fluorescence spectra of bacteriochlorophylls, its spectrum will be red-shifted from the photobleaching spectrum. Hence, the 'photobleaching' observed at the longer wavelengths (Figs. 1 and 2) actually stems from a combination of photobleaching and stimulated emission. Our treatment implicitly assumes that the spectra observed at the earliest times (2 ps) in Fig. 2 arise from vibrationally relaxed excited states. The main evidence in support of this hypothesis is the absence of any dynamic red shifts (arising from vibrational relaxation in the stimulated emission component) in our photobleaching spectra.

BChl c monomer absorption will also contribute to the total absorption difference spectrum. We are aware of few accurate measurements of BChl or Chl monomer excited state spectra so that monomer absorption is not incorporated in our simulations.

Coherent exciton model for difference absorption spectra

In Fig. 6, we summarize model calculations for the absorption difference spectra under contrasting assumptions about the exciton dynamics for J-aggregates and for chiral aggregates with the transition moment distribution given by Eqn. 7. It is assumed throughout that the BChl c excitations are coherent electronic states delocalized over N chromophores. Here the monomer spectrum is modeled as a Gaussian lineshape, with fwhm adjusted to yield an absorption difference spectrum with the experimental ratio of signals at 720 and 740 nm (Fig. 2). The exciton coupling β was

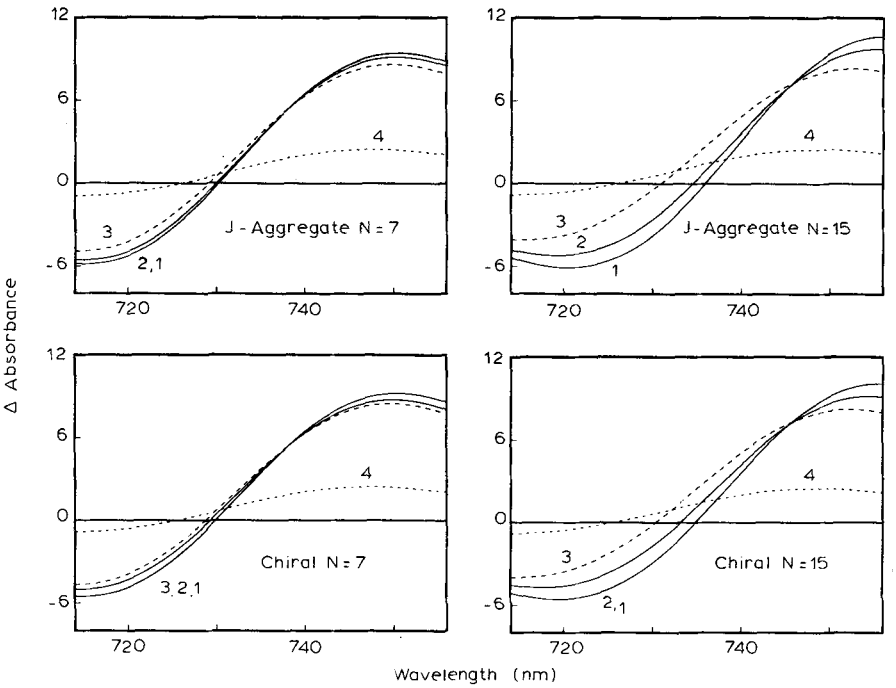

Fig. 6. Simulations of difference absorption spectra for J-aggregates ($\phi = 0$) and for chiral aggregates with $\theta = 17°$ and $\phi = 20°$. Cases are illustrated for $N = 7$ and $N = 15$. Prompt spectra are shown for excitation at (1) 750 nm and (2) 720 nm. The spectra labeled (3) are for 300 K Boltzmann distributions of excitation among the exciton components, spectra labeled (4) are for excitations localized on single chromophores.

obtained by equating 2β with the energy shift between the 670 and 740 nm BChl c chlorosome and monomer bands; this gave $\beta = -765$ cm^{-1} and -730 cm^{-1} for $N = 7$ and 15, respectively. For the chiral aggregates, θ was assumed to be 17°, the maximum angle consistent with linear dichroism studies [10,11]; the azimuthal step angle ϕ was given the largest value (20° C) that appears to be consistent with circular dichroism spectra [10]. The stimulated emission band for each exciton component was represented by a Gaussian lineshape, with fwhm and height identical to those of the corresponding photobleaching lineshape. Since fluorescence spectra of bacteriochlorophylls are red-shifted by approx. 10 nm from the absorption maxima, each stimulated emission band was assigned a 180 cm^{-1} red shift with respect to the photobleaching band.

Among the simulated spectra in Fig. 6 are prompt (unrelaxed) difference spectra for excitation at 720 and 750 nm (curves 2 and 1, respectively), and spectra that were computed by allowing the excitation level populations to reach thermal equilibrium at 300 K (curve 3). Four sets of these spectra are shown, for chiral aggregates and J-aggregates with $N = 7$ and 15. The spectra for larger N nearly coincide with those for $N = 15$. These simulations illustrate that the prompt spectra are comparatively insensitive to excitation wavelength between 720 and 750 nm. In each case, the thermalized spectrum is blue-shifted from the prompt spectra. While these blue shifts are small (≤ 1 nm) for $N = 7$, they become comparable to the experimental shift of approx. 4 nm for $N \geq 15$. There is little difference here between the simulations for J-aggregates and chiral aggregates.

The pertinent exciton domain size N for chlorosomes is unknown, and even the physical size of BChl c aggregates in the rodlike elements is uncertain. The rods are resolvable under electron microscopy [1], and likely contain many more than ten chromophores; a chlorosome contains some 10^4 BChl c monomers. De Boer and Wiersma [31] studied the dephasing-induced damping of superradiance in J-aggregates of pseudoisocyanine bromide (PIC-Br) in ethylene glycol/water glass as a function of temperature. Such J-aggregates are believed to encompass on the order of 50000 chromophores [32]. These measurements indicated that the radiative decay rate scaled essentially linearly with $1/T$ between 40 and 220 K. The estimated effective exciton domain sizes were $N_{\text{eff}} = 115$ to 650 at 40 K, and $N_{\text{eff}} = 10$ to 54 at 220 K (the matrix glass point). The domain size N_{eff} yielded by such radiative lifetime measurements is smaller than the number N of coherently coupled molecules, owing to pure dephasing processes that reduce the effective transition dipole of the lowest singly excited exciton component [31]. Extrapolation of de Boer and Wiersma's results to 300 K would project radiative domain sizes N_{eff} of 4 to 20 at room temperature; these would be lower limits to the actual coherence domain size N. In our exciton stimulations of the absorbance difference spectra, domain sizes as low as $N = 15$ are sufficient to produce the observed blue shifts.

Localized excitation model

It is also possible to simulate bipolar absorption difference spectra by assuming that the coherent states have evolved into excitations localized on single chromophores. In this case, the 'excited state' absorption spectrum is simply computed by considering transition to the exciton levels that can be reached from the $(N-1)$ unexcited chromophores, and by assuming that the position of the localized excitation is randomly distributed along the aggregate. In this picture, the blue shift between the ground state and 'excited state' spectra arises simply from the smaller effective aggregate sizes for interaction with the second photon. These spectra are shown by curve 4 for each of the cases in Fig. 6. The differences between these localized spectra and the prompt spectra model the spectral changes that would accompany the localization of the initially prepared coherent states at single chromophores. Like the previous simulations for relaxation between coherent exciton components (solid curves in Fig. 6), this calculation correctly predicts a dynamic blue shift (~ 3 nm for $N=7$, and ~ 8–10 nm for $N=15$). Moreover, it successfully predicts an experimental feature in Fig. 2 that is lacking in the coherent model: the ratio of the signals at 755 and 720 nm increases with time. Fig. 6 also predicts that the total bipolar absorption difference signal would decline sharply during such a localization process; this arises from extensive cancellation between the excited state absorption and photobleaching bands, which prove to be more closely spaced in the localized than in the coherent model. This would be reflected by the appearance of short lifetime component(s), commensurate with the 7 ps blue-shifting kinetics, in the isotropic decay.

Finally, we consider the extreme case where excitation localization is essentially complete by 2 ps. If the BChl *c* pigments are spectroscopically homogeneous, no spectral shifting would occur in the absence of exciton coupling. Thermalization of electronic excitation among energetically distinct ' pigment pools' would not be expected to cause the observed blue shift. The occurrence of blue-shifting therefore suggests that exciton coherence is maintained for at least approx. 7 ps after excitation. It is difficult to see how exciton localization would produce the fluorescence red shift observed by Holzwarth et al. [7]: the lowest exciton component (which carries most of the dipole strength in a linear aggregate) lies considerably below the monomer Q_y state. Hence, relaxation between exciton components appears to be the most likely origin for both our dynamic blue shift and the dynamic red-shift observed in the BChl *c* fluorescence spectrum of BChl *a*-free chlorosomes [7]. The red shifts could not be resolved in the fluorescence decay-associated spectra of BChl *a*-containing chlorosomes [7], so that the present experiment appears to be the first observation of BChl *c* spectral shifting in the latter type of preparation. The 7 ps lifetime associated with our dynamic blue shifts (Fig. 3) is similar to the 5 ps lifetime found by Holzwarth and coworkers in their fluorescence red shift kinetics for BChl *a*-free chlorosomes. The latter group offered two mechanisms for these red shifts (downhill EET between different pigment pools, versus relaxation between different exciton components). The first of these explanations appears to be inconsistent with our observation of the time-dependent blue shift, because it would likely cause a red shift in the pump-probe as well as fluorescence experiments.

It is important to emphasize here that the qualitative absorption difference spectra (and blue shift) modeled in Fig. 6 are not unique to the translational symmetry or ordering in the linear exciton model. Analogous phenomena can be predicted using similar exciton models for the circular aggregates that have been proposed for the B800-850 antenna complex in purple photosynthetic bacteria, and for the less symmetric BChl *a*-protein antenna complex from the green bacterium *Prosthecochloris aestuarii* (Van Amerongen and Struve, unpublished work).

The occurrence of these dynamic blue shifts on the time scale of approx. 7 ps complicates the analysis of our isotropic decays in terms of multiexponential decay models. In the presence of blue-shifting, the time-dependent absorbance difference observed at wavelength λ assumes to a first approximation the factor $(B(\lambda) + C(\lambda)\exp(-t/7\text{ ps}))$, which must be compounded with the population decay of excitation in the BChl *c* antenna. If the latter decay is represented as a biexponential function $(D\exp(-t/\tau_1) + E\exp(-t/\tau_2))$ with lifetimes $\tau_1 \sim 11$ and $\tau_2 \sim 27$ ps as suggested in earlier work [7], the difference absorption in the presence of blue-shifting becomes

$$\Delta A(\lambda, t) = (B + C\,e^{-t/7})(D\,e^{-t/11} + E\,e^{-t/27})$$

$$= BD\,e^{-t/11} + BE\,e^{-t/27} + CD\,e^{-t/4.3} + CE\,e^{-t/5.6} \quad (11)$$

where all of the lifetimes are in ps. Hence, this model predicts clustering of at least three lifetime components in the regime between 4.3 and 11 ps, and these will not be readily resolved even in a global analysis. The lifetime fitting parameters in Table I indicate, moreover, that this kinetic model is oversimplified. For example, the parameter $C(\lambda)$ is relatively small at 715 to 720 nm, so that according to Eqn. 11 the early-time decay here should be dominated by an 11 ps lifetime. However, the large-amplitude fast component lifetimes at 715 to 720 nm are found to be $\sim$ 3 ps and $\sim$ 1–2 ps in the biexponential and triexponential fits, respectively. Consequently, an additional fast component (arising from an unidentified process) exists at short wavelengths that is not accounted for by this model.

On the other hand, the moderately fast component lifetimes (3–4 ps) observed at wavelengths longer than 735 nm are consistent with the model. The intermediate lifetime components (10–15 ps) found in our triexponential fits at wavelengths between 740 and 750 nm resemble the major 11 ps component identified in the 750 nm photobleaching decay by Gillbro and coworkers [8]. Our long components at these wavelengths may correspond to their 350 ps component; the accuracy of our triexponential fits is limited here by the small amplitudes in these components and by the fact that our pump-probe scan durations were approx. 50 ps. Our biexponential fits consistently converge to a long-component lifetime of ~ 40 ps, which is similar to the intermediate component observed in the 750 nm pump-probe study [8]. The present work thus suggests that an accurate description of the overall BChl *c* excited state kinetics would require several lifetime components between 3 and 10 ps, and additional components at approx. 10–15, 30–40 and over 100 ps. We cannot rule out exciton annihilation as one of the decay channels in the overall isotropic kinetics. We have mentioned earlier that approximately one of every 100 BChl *c* chromophores is excited at the 740 nm peak wavelength. Vos et al. [26] estimated that at 4 K, this number of BChl *c* molecules corresponds to the annihilation domain size. The possibility of doubly exciting a single domain, accompanied by rapid singlet-singlet annihilation, may thus provide an additional rapid route for isotropic decay if the domain size is not smaller than ~ 100 chromophores at room temperature. Most of our decay components, however, can be explained by compounding the 7 ps blue shift with the 11 and 27 ps lifetime components observed elsewhere [7].

Pending farther clarification of the three-dimensional structure of the BChl *c* aggregates in chlorosomes, the interpretation of the anisotropic decays (Fig. 4) remains speculative. Depolarization can arise from relaxation between exciton components in the (presumably) linear aggregates, since different exciton components will exhibit contrasting expansion coefficients in the monomer states (cf. Eqn. 4) and the transition moment architecture is known to be chiral. In this context, the similarity between the lifetimes associated with the dynamic blue shift and the depolarization at 720 nm (both ~ 7 ps) is interesting. Other conceivable mechanisms for depolarization are excitation hopping between different exciton domains within the same BChl *c* aggregate, and even energy transfer between different rodlike BChl *c* elements in the chlorosome. More than one physical process may contribute to the observed depolarization, because the difference between our measured depolarization lifetimes at 720 and 740 nm (~ 7 and 4 ± 1 ps, respectively) appears to be larger than experimental error. This situation is reminiscent of an earlier observation that the wavelength dependence of the depolarization lifetime in photobleaching of Chl *a* antennae in photosystem I correlates inversely with the ground state absorption spectrum [29].

The fact that the residual anisotropy $r(\infty)$ is larger at 740 than at 720 nm (Fig. 4) is consistent with the theory of linear excitons in chiral aggregates. If the transition moment orientations for each of the N chromophores j in the aggregate are modeled as in Eqn. 7, the polarized intensities for ground-state transitions to exciton component i are then given by

$$A_{ix} = \left(\sum_{j=1}^{N} c_{ij}\mu_{jx}\right)^2 = \frac{2}{N+1}\left[\sum_{j=1}^{N} \cos j\phi \sin\left(\frac{ij\pi}{N+1}\right)\right]^2 \sin^2\theta \quad (12a)$$

$$A_{iy} = \frac{2}{N+1}\left[\sum_{j=1}^{N} \sin j\phi \sin\left(\frac{ij\pi}{N+1}\right)\right]^2 \sin^2\theta \quad (12b)$$

$$A_{iz} = \frac{2}{N+1}\left[\sum_{j=1}^{N} \sin\left(\frac{ij\pi}{N+1}\right)\right]^2 \cos^2\theta \quad (12c)$$

where we have used the expansion coefficients from Eqn. 5. In the special case of the *J*-aggregate ($\phi = 0$), the linear dichroism

$$LD = \frac{A_{iz} - (A_{ix} + A_{iy})/2}{A_{ix} + A_{iy} + A_{iz}} \quad (13)$$

reduces to

$$LD = \tfrac{1}{2}(3\cos^2\theta - 1) \quad (14)$$

for absorption to any of the exciton components j. This means that the linear dichroism (and hence the residual anisotropy) is independent of wavelength in a *J*-aggregate, in which all of the monomer transition moments are parallel. In the contrasting case of a chiral aggregate exhibiting circular dichroism ($\phi \neq 0$), the sum of the perpendicular intensities becomes

$$\begin{aligned} A_{ix} + A_{iy} &= \frac{2}{N+1}\left[\left(\sum_{j=1}^{N} \cos j\phi \sin j\phi'\right)^2 + \left(\sum_{j=1}^{N} \sin j\phi \sin j\phi'\right)^2\right] \sin^2\theta \\ &= \frac{2}{N+1}\left(\sum_{j=1}^{N} \sin^2 j\phi' + \sum_{j_1=1}^{N-1}\sum_{j_2>j_1}^{N} 2\cos[(j_1 - j_2)\phi]\sin j_1\phi' \sin j_2\phi'\right) \sin^2\theta \end{aligned} \quad (15)$$

where we define $\phi' = i\pi/(N+1)$. In the lowest exciton level (where $i = 1$ and $\sin(j_1\phi')\sin(j_2\phi')$ is therefore nonnegative-definite), the largest value of $(A_{1x} + A_{1y})$ occurs when $\phi = 0$ (i.e., when $\cos(j_1 - j_2)\phi = +1$). The lowest exciton component exhibits smaller values of $(A_{1x} + A_{1y})$ than this when $\phi \neq 0$. Since we have the conservation rules

$$\sum_{i=1}^{N} A_{iz} = N\cos^2\theta$$

and

$$\sum_{i=1}^{N} (A_{ix} + A_{iy} + A_{iz}) = N$$

it follows that the sum of perpendicular intensities

$$\sum_{i=1}^{N} (A_{ix} + A_{iy}) = N\sin^2\theta$$

is independent of the chiral angle ϕ. Increasing ϕ therefore redistributes the perpendicular intensities from the lowest exciton component to higher exciton components. Eqn. 15 then predicts that chiral aggregates will exhibit linear dichroism that increases with wavelength, in agreement with our finding that the residual anisotropy $r(\infty)$ is larger at 740 than at 720 nm. These results become modified in the presence of excited state absorption, which dominates at 720 nm (Fig. 2). A quantitative calculation based on the chiral aggregate model with $N = 10$, $\theta = 17°$ and $\phi = 20°$ predicts that the residual anisotropy $r(\infty)$ increases from 0.30 to 0.32 between 720 and 740 nm. This simple model thus underestimates the change in $r(\infty)$ by a factor of 2 to 4. Such a wavelength effect can be difficult to establish in steady-state linear dichroism studies in aggregates with small chiral angles ϕ, but it was observed by Griebenow et al. [10]. Since the residual anisotropy $r(\infty)$ is proportional to the square of the steady-state linear dichroism, pump-probe experiments are potentially a more sensitive method for detecting chirality effects in linear dichroism.

Conclusions

In summary, our pump-probe experiments on BChl *a*-containing chlorosomes from *C. aurantiacus* have identified the following features in the BChl *c* difference absorption spectra:

(1) The isotropic spectrum between 715 and 755 nm is bipolar, exhibiting photobleaching and excited-state absorption at longer and shorter wavelengths respectively. It is in qualitative agreement with earlier spectra observed in chlorosomes from *C. aurantiacus* and *C. limicola* [26], and it resembles the transient difference spectrum of Chl *a* dihydrate oligomers in solution [33]. This spectrum can be modeled with linear exciton calculations of BChl *c* ground-state photobleaching, excited state absorption, and stimulated emission.

(2) The entire isotropic spectrum experiences a dynamic blue shift during the first approx. 7 ps. This can be rationalized in terms of relaxation between exciton components in the linear exciton theory, and its time scale is similar to that of a BChl *c* fluorescence red shift observed in BChl *a*-free chlorosomes by Holzwarth et al. [7]. The occurrence of the blue shift is not readily explained in terms of downhill EET between BChl *c* pigment pools. A third explanation, exciton localization, appears to be inconsistent with the fluorescence red shift.

(3) Analysis of the isotropic decay profiles obtained with 2 ps resolution indicates that they are not adequately modeled at all wavelengths using a triexponential decay law. There appear to be several lifetime components clustered between 3 and 10 ps, in addition to the components at 10–15, 30–40 and over 100 ps reported by other groups [7,8].

(4) The anisotropy decay times, which depend on the probed wavelength, are 7 ± 1 ps at 720 nm and 4 ± 1 ps at 740 nm. The anisotropy functions $r(t)$ extrapolate to $r(0) = 0.4$ within error, indicating that subpicosecond depolarization is not a major process. The residual anisotropy $r(\infty)$ is 0.32 ± 0.02 at 740 nm; this value is good agreement with prior fluorescence and linear dichroism measurements [10–13]. The residual anisotropy is lower at 720 nm (0.24 ± 0.02); this wavelength trend in $r(\infty)$ is consistent with the exciton theory for linear dichroism in chiral aggregates.

Acknowledgements

The Ames Laboratory is operated for the U.S. Department of Energy by Iowa State University under Contract No. W-7405-Eng-82. This work was supported by the Division of Chemical Sciences, Office of Basic Energy Sciences. We are particularly indebted to Alfred Holzwarth for providing the chlorosome samples.

Note added in proof (Received 5 August 1991)

Recent spectral hole-burning measurements on the BChl *c* absorption bands in whole cells of *C. limicola* and *C. aurantiacus* have shown that the inhomogeneous broadening is on the order of 100 cm^{-1} in both antennae (Fetisova, Z.G., personal communication). This is similar to the magnitude of the dynamic blue shift observed in our work (approx. 75 cm^{-1}). An additional possible origin of the blue shift is vibrational cooling of hot ground-state BChl *c* molecules, formed in ground-state repopulation. It has been brought to our attention that EPR studies of the BChl *c* antenna

in *C. aurantiacus* suggest that the effective aggregate size in vivo is approx. 13 [22].

References

1 Staehelin, L.A., Golecki, J.R., Fuller, R.C. and Drews, G. (1978) Arch. Microbiol. 119, 269–277.
2 Golecki, J.R. and Oelze, J. (1987) Arch. Microbiol. 148, 236–241.
3 Van Dorssen, R.J. and Amesz, J. (1988) Photosynth. Res. 15, 177–189.
4 Mimuro, M., Nozawa, T., Tamai, N., Shimada, K., Yamazaki, I., Lin, S., Knox, R.S., Wittmershaus, B.P., Brune, D.C. and Blankenship, R.E. (1989) J. Phys. Chem. 93, 7503–7509.
5 Müller, M.G., Griebenow, K. and Holzwarth, A.R. (1990) in Current Research in Photosynthesis (Baltscheffsky, M., ed.), Vol. II, pp. 4.177–4.180, Kluwer Academic Publishers, Dordrecht.
6 Causgrove, T.P., Brune, D.C., Wang, J., Wittmershaus, B.P. and Blankenship, R.E. (1990) Photosynth. Res. 26, 39–48.
7 Holzwarth, A.R., Müller, M.G. and Griebenow, K. (1990) J. Photochem. Photobiol. B5, 457–465.
8 Miller, M., Gillbro, T. and Cox, R.P. (1990) in Current Research in Photosynthesis (Baltscheffsky, M., ed.), Vol. II, pp. 4.181–4.184, Kluwer Academic Publishers, Dordrecht.
9 Griebenow, K. and Holzwarth, A.R. (1989) Biochim. Biophys. Acta 973, 235–240.
10 Griebenow, K., Holzwarth, A.R., Van Mourik, F. and Van Grondelle, R. (1991) Biochem. Biophys. Acta, in press.
11 Van Amerongen, H., Vasmel, H. and Van Grondelle, R. (1988) Biophys. J. 54, 65–76.
12 Van Amerongen, H., Van Haeringen, B., Van Gurp, M. and Van Grondelle, R., Biophys. J., in press.
13 Fetisova, Z.G., Freiberg, A.M. and Timpmann, K.E. (1988) Nature 334, 633–634.
14 Brune, D.C., Nozawa, T. and Blankenship, R.E. (1987) Biochemistry 26, 8644–8652.
15 Lutz, M. and Van Brakel, G. (1988) in Green Photosynthetic Bacteria (Olson, J.M., Ormerod, J.G., Amesz, J., Stackebrandt, E. and Trüper, H.G., eds.), pp. 23–24, Plenum Press, New York.
16 Brune, D.C., King, G.H. and Blankenship, R.E. (1988) in Photosynthetic Light-Harvesting Systems (Scheer, H. and Schneider, S., eds.), pp. 141–151, Walter de Gruyter, Berlin.
17 Causgrove, T.P., Brune, D.C., Blankenship, R.E. and Olson, J.M. (1990) Photosynth. Res. 25, 1–10.
18 Blankenship, R.E., Brune, D.C., Freeman, J.M., King, G.H., McManus, J.D., Nozawa, T., Trost, J.T. and Wittmershaus, B.P. (1988) in Green Photosynthetic Bacteria (Olson, J.M., Olmerod, J.G., Amesz, J., Stackebrandt, E. and Trüper, H.G., eds.) pp. 57–86, Plenum Press, New York.
19 Olson, J.M. and Pedersen, J.P. (1990) Photosynth. Res. 25, 25–37.
20 Matsuura, K. and Olson, J.M. (1990) Biochim. Biophys. Acta 1019, 233–238.
21 Bystrova, M.I., Mal'gosheva, I.N. and Kranovski, A.A. (1979) Mol. Biol. 13, 440–451.
22 Smith, K.M. and Kehres, L.A. (1983) J. Am. Chem. Soc. 105, 1387–1389.
23 McRae, E.G. and Kasha, M. (1958) J. Chem. Phys. 28, 721–722.
24 Chen, S.-Y., Horng, M.-L. and Quitevis, E.L. (1989) J. Phys. Chem. 93, 3683–3688.
25 Eckhardt, A., Brunisholz, R., Frank, G. and Zuber, H. (1990) FEBS Lett. 267, 199–202.
26 Vos, M., Nuijs, A.M., Van Grondelle, R., Van Dorssen, R.J., Gerola, P.D. and Amesz, J. (1987) Biochim. Biophys. Acta 891, 275–285.
27 Feick, R.G., Fitzpatrick, M. and Fuller, R.C. (1982) J. Bacteriol. 150, 905–915.
28 Betti, J.A., Blankenship, R.E., Natarajan, L.V., Dickinson, L.C. and Fuller, R.C. (1982) Biochim. Biophys. Acta 680, 194–201.
29 Causgrove, T.P., Yang, S. and Struve, W.S. (1989) J. Phys. Chem. 93, 6844–6850.
30 Van Dorssen, R.J., Vasmel, H. and Amesz, J. (1986) Photosynth. Res. 9, 33–45.
31 De Boer, S. and Wiersma, D.A. (1990) Chem. Phys. Lettr. 165, 45–33.
32 Sundström, V., Gillbro, T., Gadonas, R.A. and Piskarskas, A. (1988) J. Chem. Phys. 89, 2754–2762.
33 Maly, P., Danelius, R. and Gadonas, R. (1987) Photochem. Photobiol. 45, 7–11.